INSTITUTO DE ASTRONOMIA, GEOFÍSICA E CIÊNCIAS ATMOSFÉRICAS

Conselho Nacional de Desenvolvimento Científico e Tecnológico

Interstellar observations of HNCO

a potential precursor of prebiotic molecules

Carla M. Canelo (IAG)

E. Mendoza (IAG), A. C. S. Friaça (IAG) et al.

Astrochemistry LLAMA Meeting - São Paulo, BR - August, 2019

Scientific Case

HNCO as a prebiotic molecule

- Contains four of the biogenic elements (CHONPS)

- Observed in comets, protostellar regions and clouds.

- The peptide link (–NH–C(=O)–) play an important role in the synthesis of amino acids and proteins

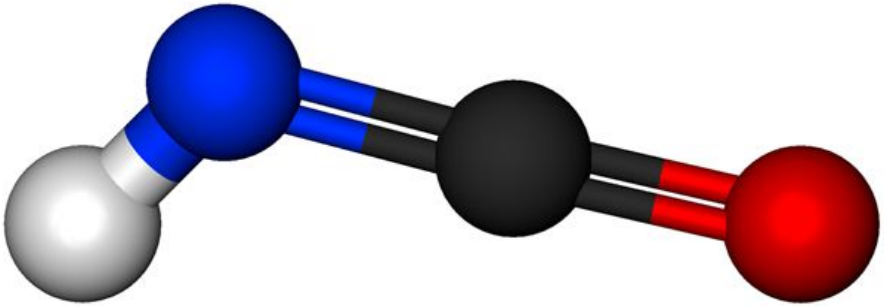

HNCO as a prebiotic molecule

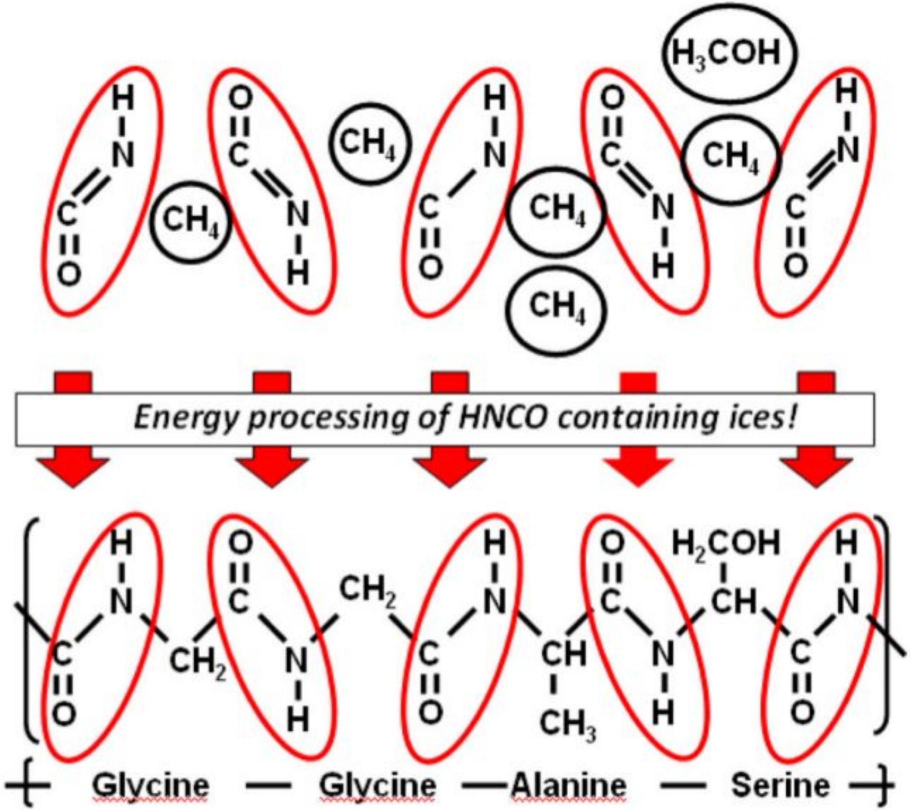

Figure 6. A schematic that illustrates the potential importance of HNCO as a simple bearer of peptide bonds for the production of amino acids in interstellar ices.

- Can form molecules with peptide bonds in solid state

- Glycine (Mendoza talk)

Fedoseev et al. 2015

HNCO and OCN-

$$
\begin{array}{ll}
\text{(i)} & HCCC + NH_2 \rightarrow C_3H_3N \\
\text{(ii)} & C_3H_3N + NH \rightarrow C_3N_2H_4 \\
\text{(iii)} & \boxed{C_3N_2H_4 + HNCO \rightarrow C_4N_3H_5O} \\
(iv) & C_4N_3H_5O + H \rightarrow C_4N_3H_6O \\
\text{(v)} & C_4N_3H_6O + NH \rightarrow C_4H_5N_3O + NH_2 \\
\text{(vi)} & C_4N_3H_6O + OH \rightarrow C_4H_5N_3O + H_2O \\
\text{(vii)} & C_4N_3H_6O + NH_2 \rightarrow C_4H_5N_3O + NH_3 \\
\hline
\text{(viii)} & \boxed{HCCCN + OCN^- \rightarrow C_4N_2OH} \\
\text{(ix)} & C_4N_2OH + H \rightarrow C_4N_2H_2O \\
\text{(x)} & C_4N_2H_2O + NH \rightarrow C_4N_3H_3O \\
\text{(xi)} & C_4N_3H_3O + H \rightarrow C_4N_3H_4O \\
\text{(xii)} & C_4N_3H_4O + H \rightarrow C_4N_3OH_5 \\
\text{(xiii)} & C_4N_3OH_5 + H \rightarrow C_4N_3H_6O \\
\text{(xiv)} & C_4N_3H_6O + H \rightarrow C_4H_5N_3O + H_2
\end{array}
$$

- could participate of the formation of cytosine in ice phase (Majumbar et al. 2015)
- could form amino acids and their anions (Fedoseev et al. 2015)

$$
\boxed{
\begin{array}{ll}
\text{(xv)} & HNCO + H \rightarrow HNCHO \\
\text{(xvi)} & HNCO + H \rightarrow NH2CO \\
\text{(xvii)} & HNCO + NH_3 \rightarrow OCN^- + NH_4{}^+ \\
\text{(xviii)} & HNCO + H_2O \rightarrow OCN^- + H_3O^+
\end{array}
}
$$

Formation of HNCO in ices

$$\boxed{NH + CO \rightarrow HNCO}$$

$$NH_2 + CO \rightarrow HNCO + H$$

$$N + CO \rightarrow NCO$$

$$H + NCO \rightarrow HNCO$$

- Gas phase reactions do not reproduce the observations

- Interstellar ice analogues processed by proton or UV radiation

Fedoseev et al. 2015

- HNCO may be correlated with **formamide**

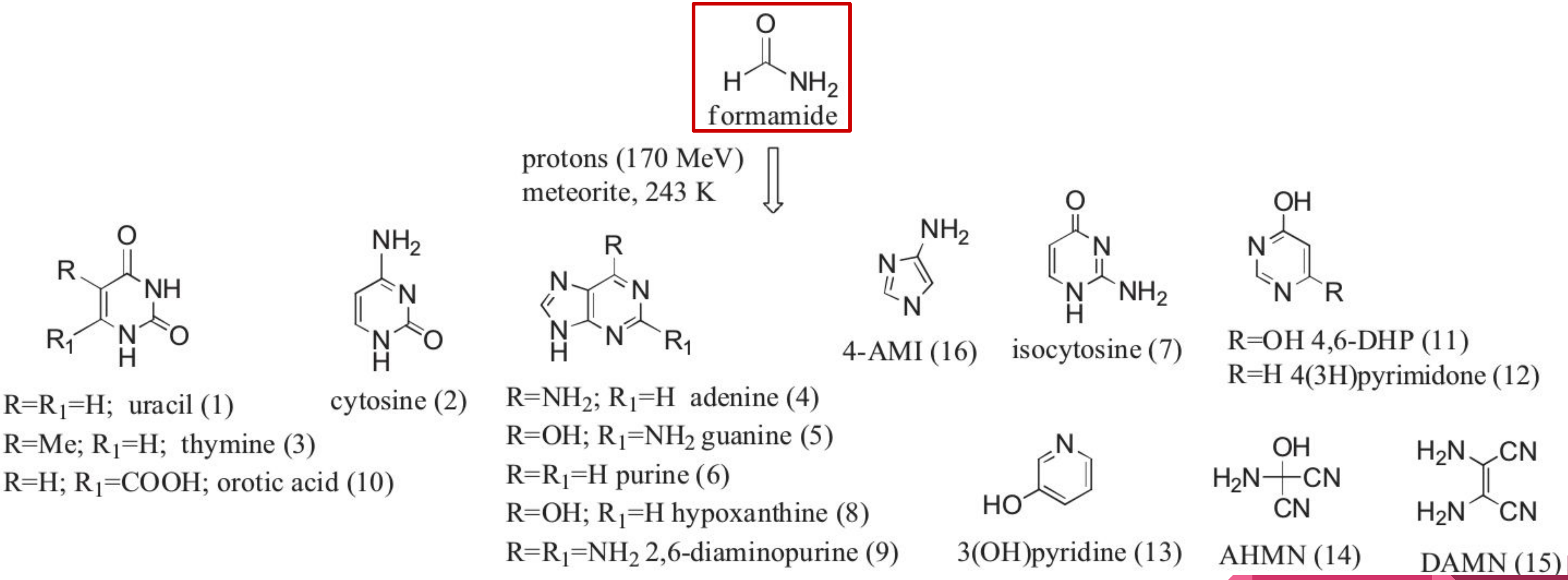

Fig.: Products of high-energy proton irradiation of formamide in the presence of meteorites. Nucleobases, nucleobase analogs, and intermediates of the condensation (Saladino et al; 2015).

HNCO and NH2CHO

- They may share a common solid state formation scheme;
    - similar conditions during ice formation
    - balance between formation and destruction in ices

- [HNCO]/[NH2CHO] ~ 3.0

Mendoza et al. 2014

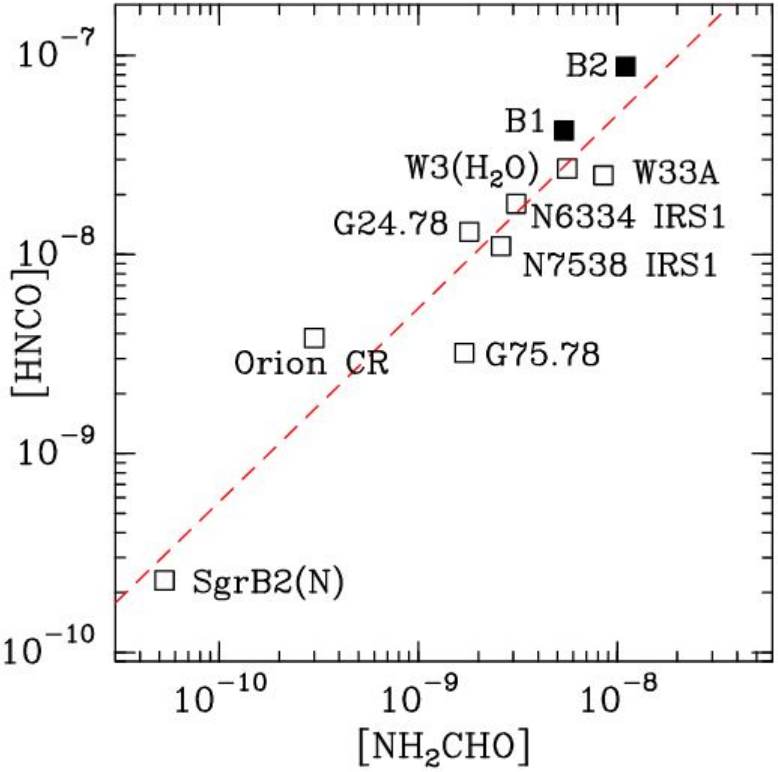

Figure 7. Comparison of molecular abundances for NH_2CHO and HNCO in a sample of Galactic sources. Filled symbols indicate our values measured towards the protostellar shocks B1 and B2. The data were taken from by Jackson, Armstrong & Barrett (1984), Sutton et al. (1995), Bisschop et al. (2007), Martín et al. (2008), and Halfen et al. (2011). The best power-law fit $[HNCO] = 3.0 \times [NH_2CHO]^{0.97}$ is drawn in dashed.

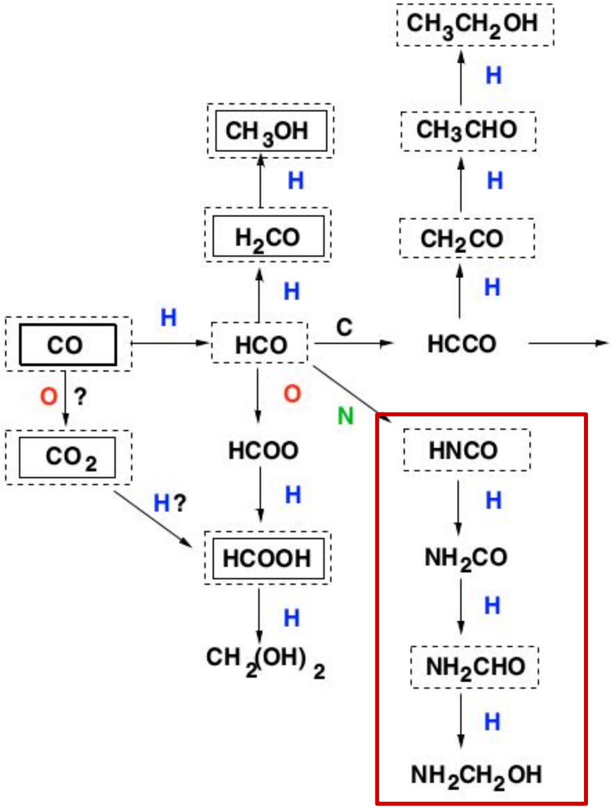

Fig. 1. Grain-surface chemistry routes involving hydrogenation of CO. Solid rectangular boxes contain molecules which have been detected in interstellar ices, whereas dashed boxes indicate molecules that have been detected in the gas phase (based on Tielens & Charnley 1997).

Grain-surface routes

- Hydrogenation of HNCO involves a activation barrier

- They may not be chemically related

Bisschop et al. 2007

CH4:HNCO ice

T=20 K

far-UV photons

(Ligterink et al. 2018)

*hydrogenation of HNCO is unlike to form NH2CHO

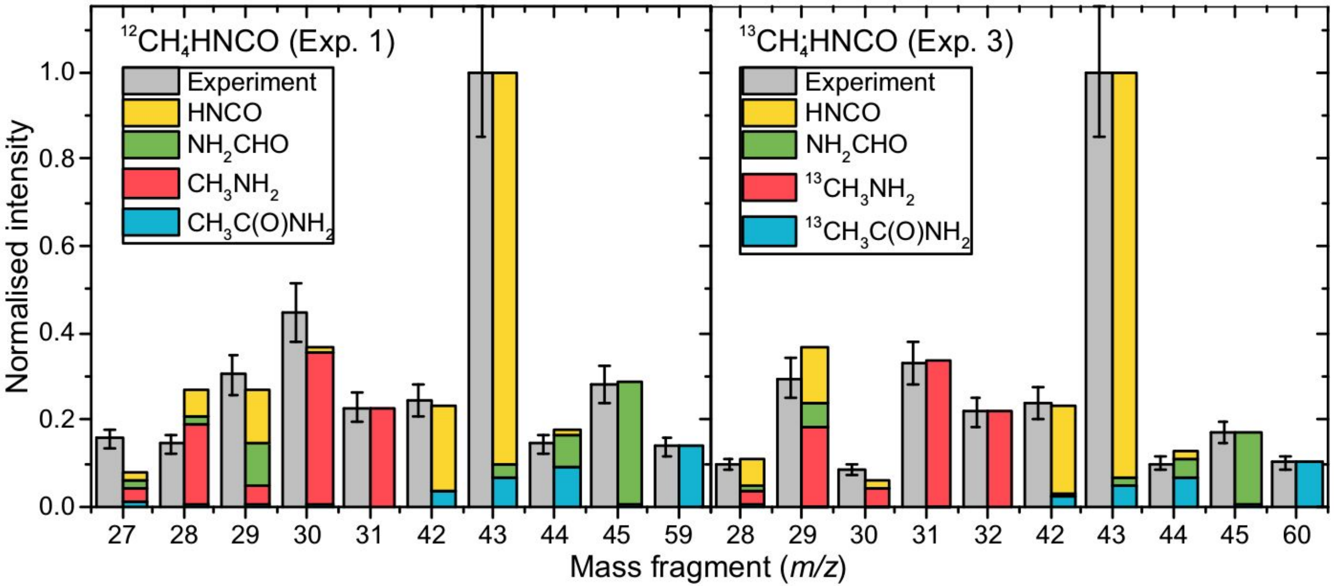

Figure 7. The fragments at *m*/*z* 60/59, 45, 44, 43, 42, 32/31, 31/30, 30/29, 29/28, and 28/27 found desorbing around 210 K in experiments 1 and 3 (black), fitted with the combined fragmentation patterns of $^{12/13}$acetamide (blue), $^{12/13}$methylamine (red), formamide (green), and HNCO (yellow). Note that intensity ratios do not directly reflect ARs.

Observation of HNCO in the Hot Molecular Core G331.512-0.103

G331.512-0.103

Hot molecular core

- ~7.5 kpc
- outflow with 55 $M_{\odot}$
- $n(H_2) \approx 2 \times 10^7\ cm^{-3}$
- $HC_3N \rightarrow T_{kin} \sim 90$ K

(Duronea et al. 2019, accepted)

$CH_3CN \rightarrow T_{kin} \sim 141$ K

$CH_3OH \rightarrow T_{kin} \sim 74$ K

(Mendoza et al. 2018)

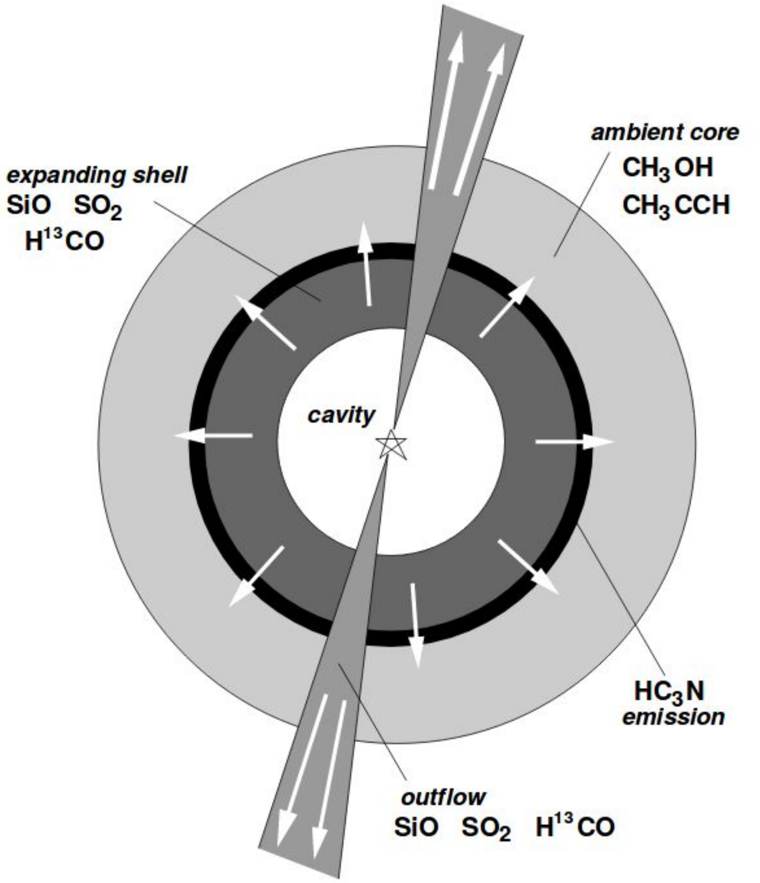

Figure 8. Sketch of the simple model proposed to explain the emission of HC_3N and other molecules detected in G331 (based on the models of Merello et al. 2013a and Hervías-Caimapo et al. 2019).

G331.512-0.103

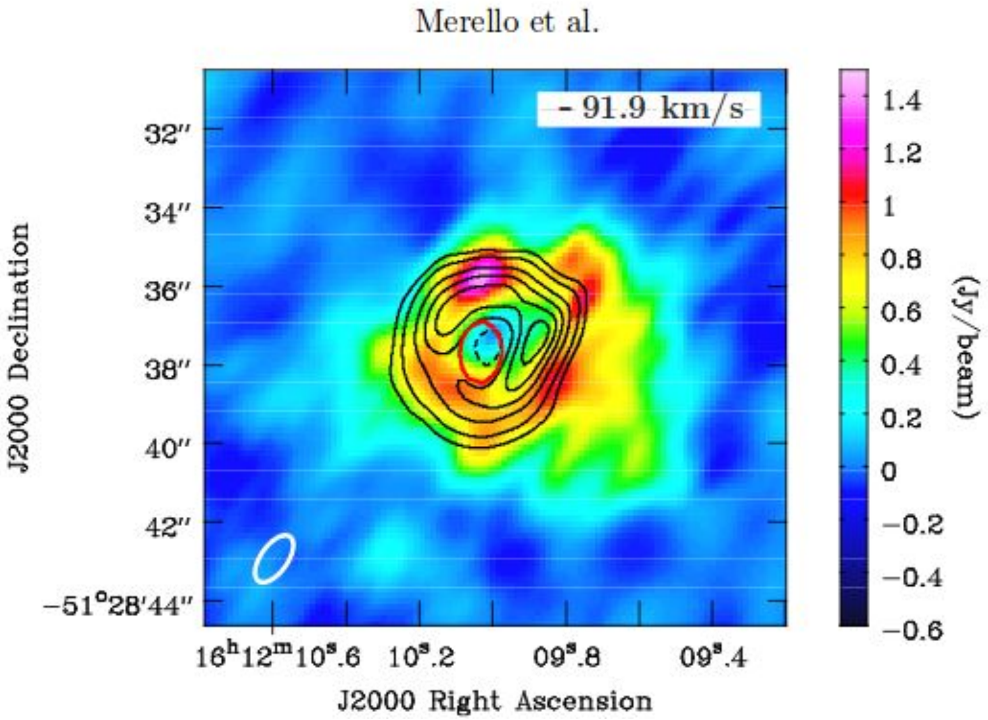

H13CO+(4-3) emission (in colors) of the G331.512−0.103 source at a velocity of−91.9 km s−1, where the peak of fluxdensity is found. The overlaid contours in black correspond to the SiO(8-7) emission at the same velocity, at 3, 6, 12, 18, 24 and 30σ(withσ=0.14 Jy beam−1)

Observed with APEX
(Atacama Pathfinder Experiment)

- APEX 1→ 213 – 275 GHz
- APEX 2 → 267 – 378 GHz

HNCO emission lines

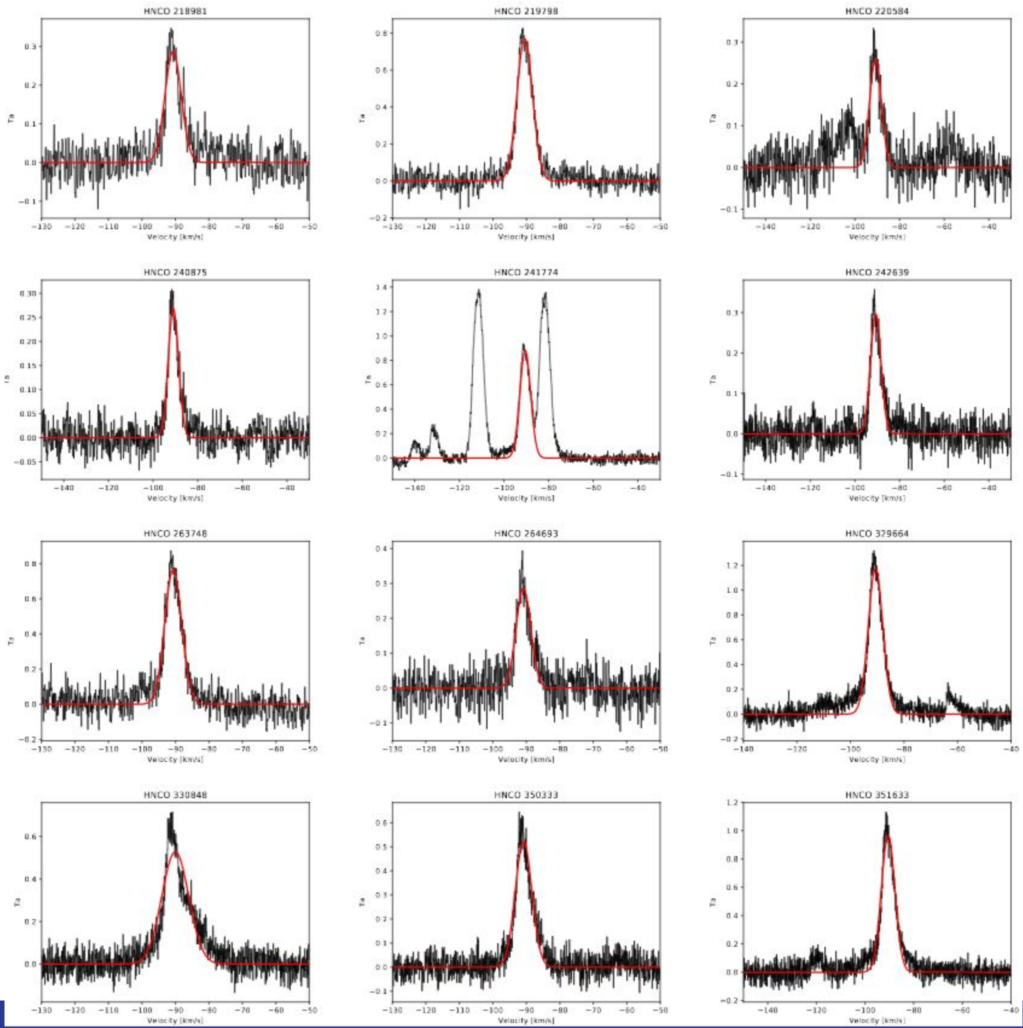

Line (MHz)	RMS	Tpeak
218981.02	0.03727	0.28763
219798.28	0.04144	0.7699
220584.76	0.03523	0.25838
240875.74	0.02328	0.26812
241774.04	0.03457	0.87987
242639.72	0.02933	0.29657
263748.63	0.06927	0.76769
264693.67	0.04062	0.28642
329664.37	0.05027	1.1739
330848.57	0.04731	0.52818
350333.06	0.04034	0.52162
351633.26	0.04829	0.96634

(Canelo et al., in prep.)

LTE-analysis

$$\ln\left(\frac{N_u}{g_u}\right) = \ln\left(\frac{N}{Z}\right) - \frac{E_u}{kT_{\mathrm{exc}}}$$

(Goldsmith & Langer 1999)

T_{exc} = 70 ± 7 K

N = 4.7 x 10^{14} cm^{-2}

(Canelo et al., in prep.)

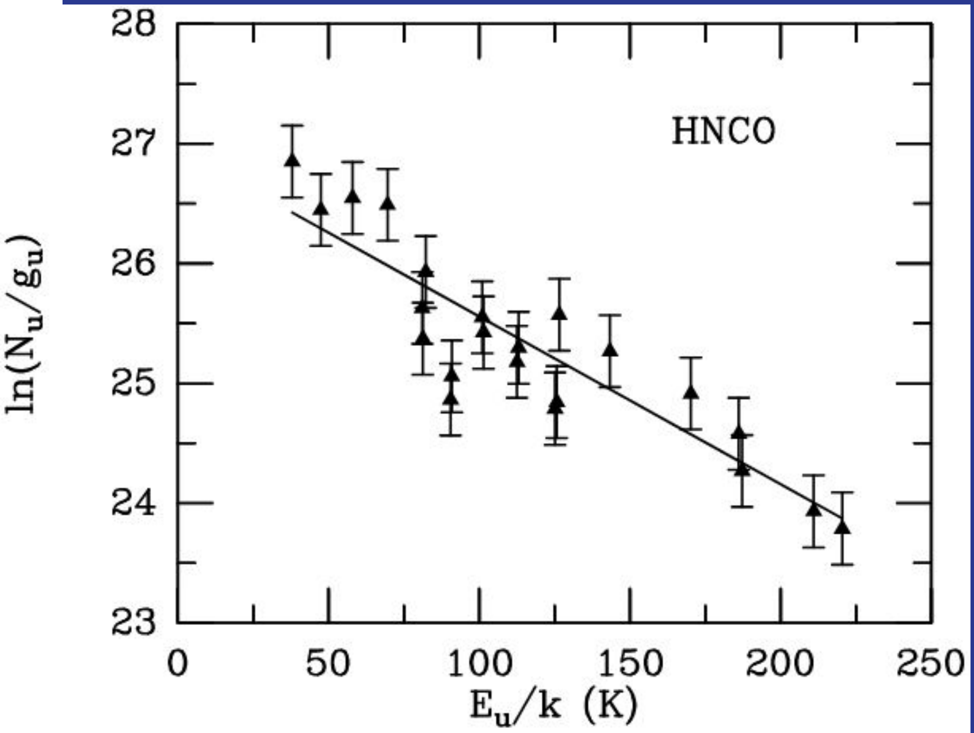

Fig. 2. Rotational diagram of HNCO. The best linear fit (χ^2_{red}=0.13) yielded T_{ex}= 70 ± 7 K and N = 4.7 × 10^{14} cm^{-2} for a beam averaged source of 15 arcsec.

Corner Diagram

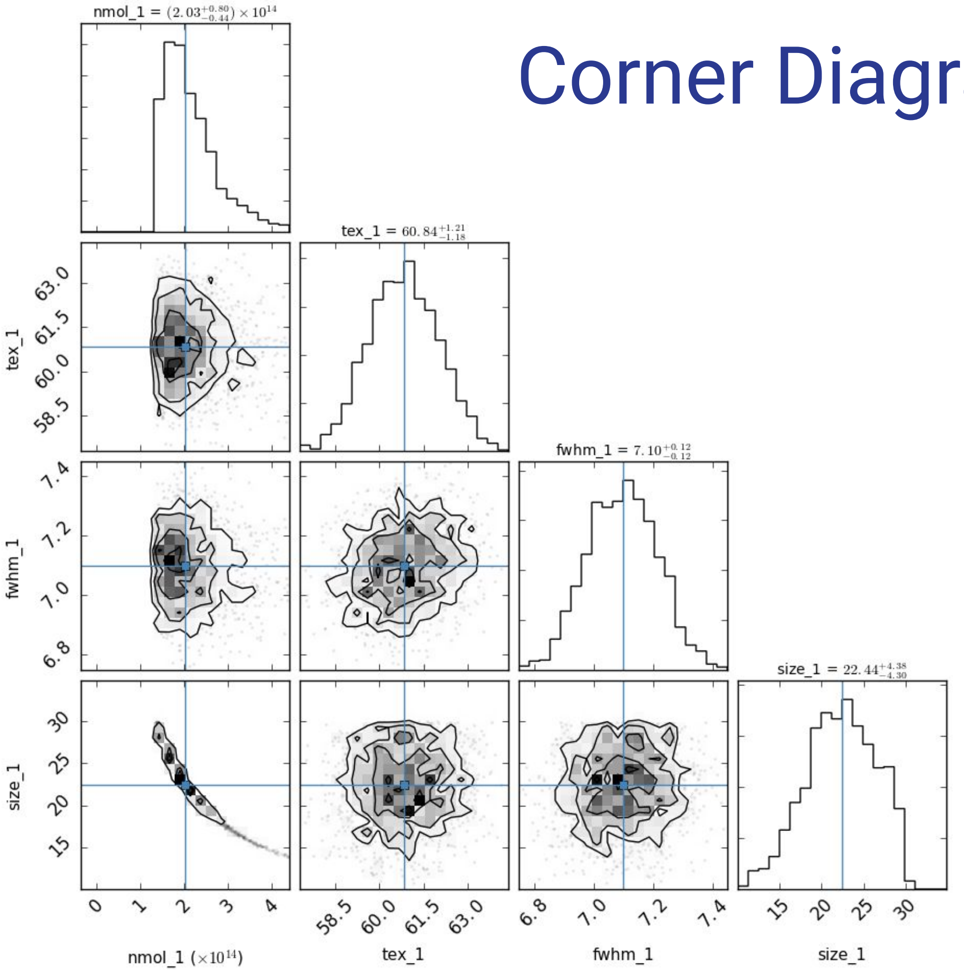

- MCMC statistical solutions for
  - Texc
  - column density

$T_{exc} \approx 61$ K

$N \approx 2 \times 10^{14}$ cm^{-2}

(Canelo et al., in prep.)

Nautilus (Ruaud et al. 2015, 2016)

- a three-phase time-dependant simulation of the chemistry (gas + grain mantle + surface)
- includes chemical reactions in both gas and solid phases
- Our simulations are zero-dimensional
  * physical conditions are uniform
- No structure evolution

Cloud initial elemental abundances (Vidal & Wakelam 2018)

Elemento	$n_i/n_H{}^a$	Elemento	$n_i/n_H{}^a$
H_2	0.5	He	9.0(-2)
N	6.2(-5)	O	2.4(-4)
C+	1.7(-4)	S+	1.5(-5)
Fe+	3.0(-9)	Si+	8.0(-9)
Na+	2.0(-9)	Mg+	7.0(-9)
Cl+	1.0(-9)	P+	2.0(-10)
F	6.7(-9)		

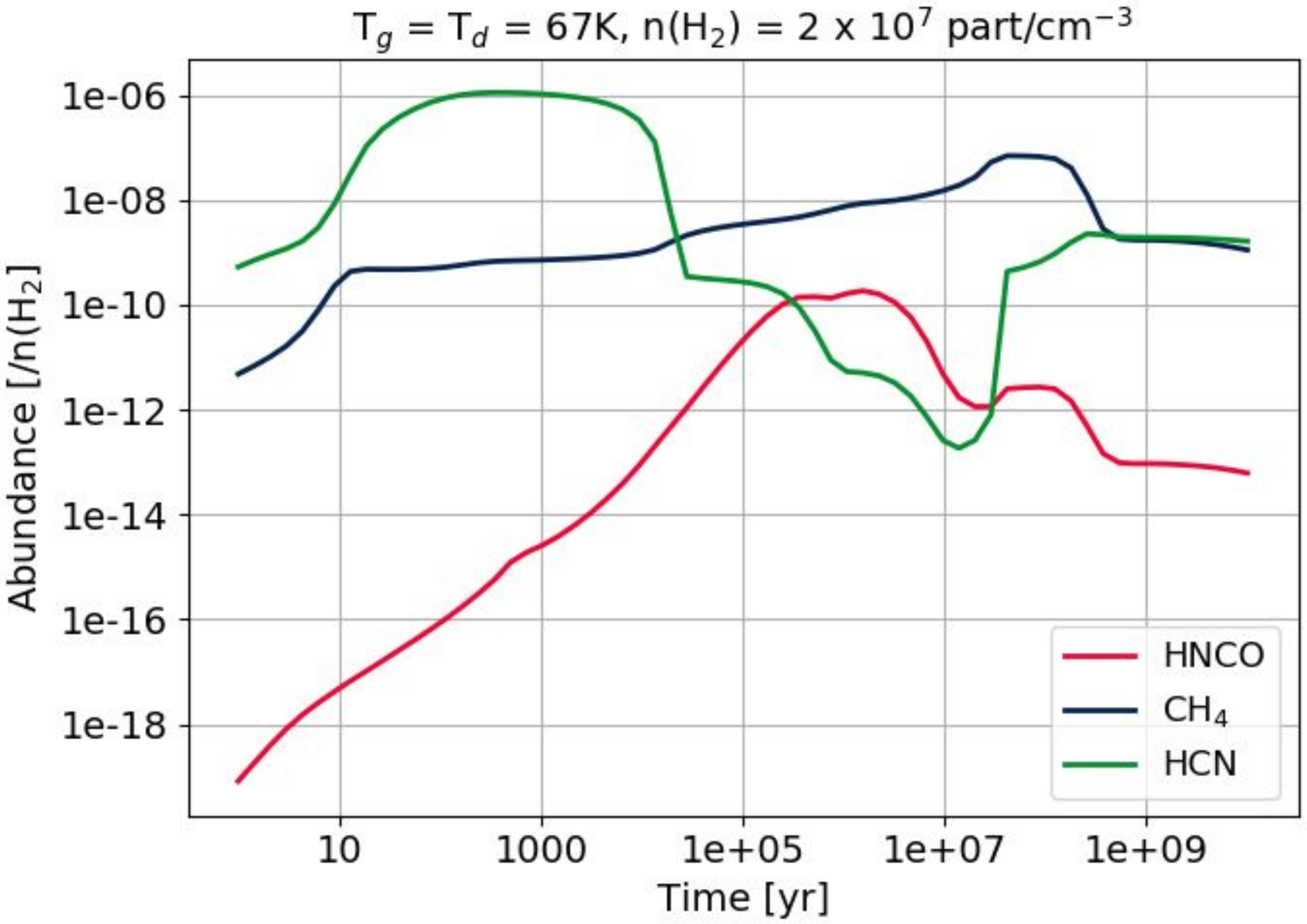

Best-fit model

A_v = 10 mag
ζ = 1.3 x 10^{-17} s^{-1}
$T_{gas} = T_{dust}$

Perspectives - LLAMA

Search for interstellar emission of N-heterocycles

Motivation → Prebiotic chemistry

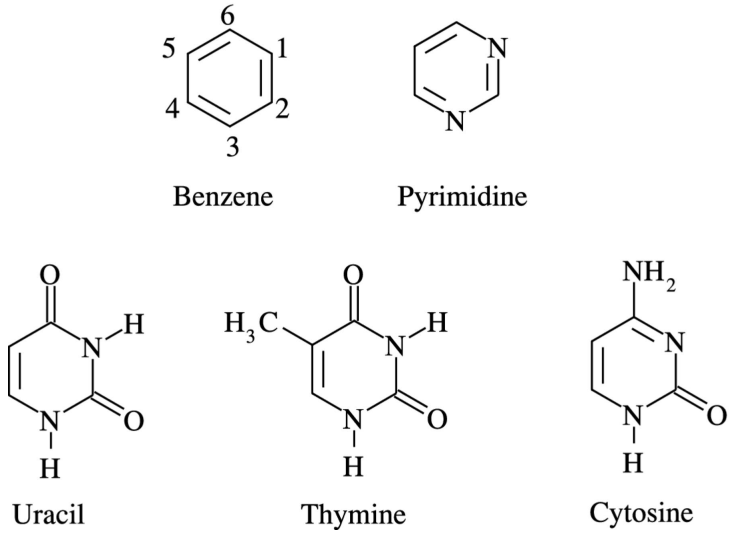

Fig.: Molecular structure of benzene, pyrimidine and pyrimidinic nucleobases uracil, thymine and cytosine (Mendoza et al. 2013).

- Formation of nucleobases
- Presence in meteorites (e.g. Murchison)

(Allamandola et al. 1999, Martins et al. 2005, 2008)

- Large dipole moments

  → detection at radio wavelengths

  (Charnley et al. 2005)

N-heterocycles detection in ISM

- Vinyl cyanide, pyrimidine and pyridine in 1973

  (Martha Simon & Michal Simon, 1973)

- Pyridine, pyrimidine, quinoline, isoquinoline

  (Charnley et al. 2005, Kuan et al. 2006)

Still a challenge:

- Low abundances
- Photodissociation

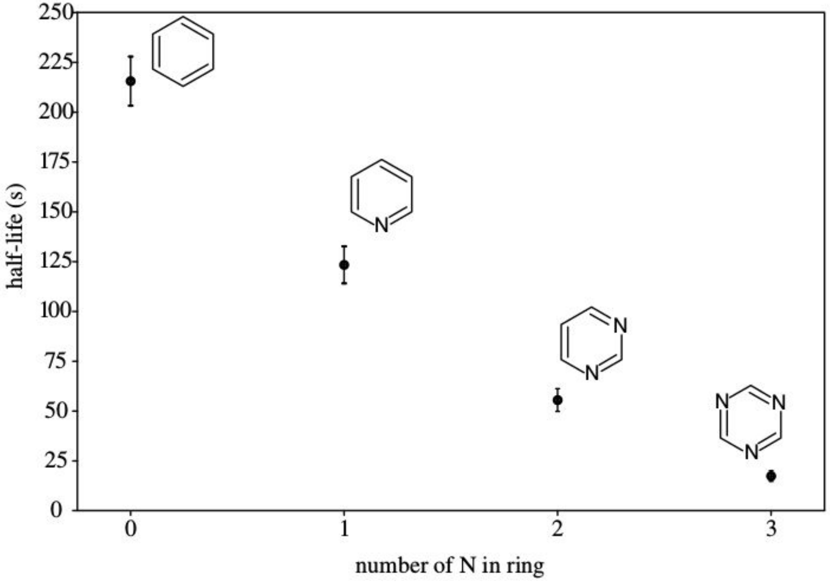

Fig.: The half-lives of the three N-heterocycles plotted against the number of nitrogen atoms in the ring. (Z. Peeters et al. 2005).

Search for N-heterocycles precursors

- HNCO, HC3N, C3H and HC3NH$^+$ (Majumdar et al. 2015)

- Formamide

- Vinyl cyanide (C2H3CN) (Parker & Kaiser, 2017)

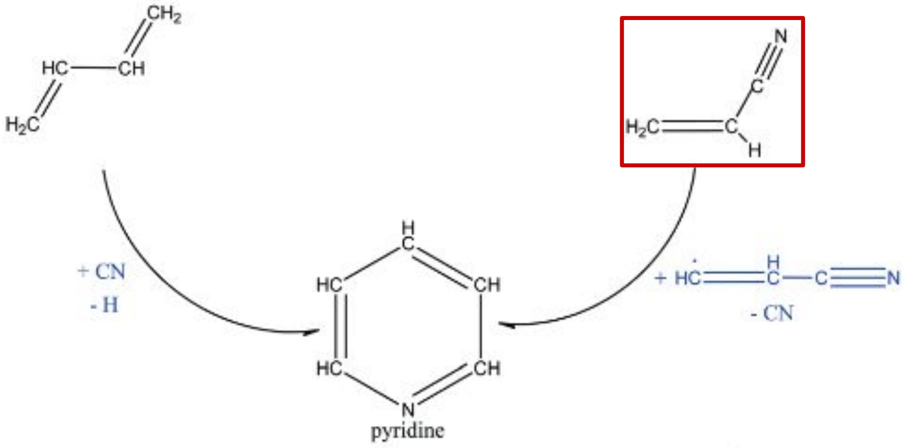

LLAMA

- BAND 5: 162 - 211 GHz

Setups centred in typical transitions to cover the frequency interval

Transitions predicted by the CDMS database: HNCO, pyrrole, pyridine

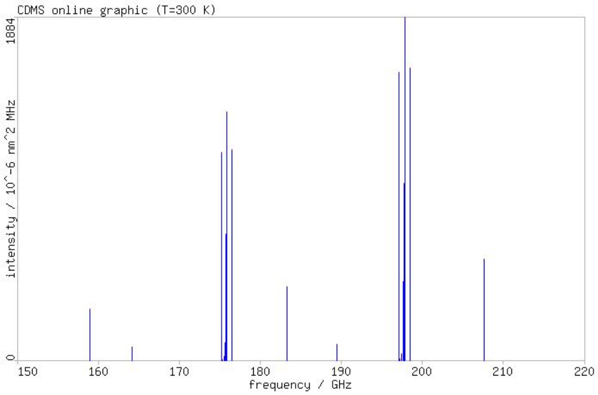

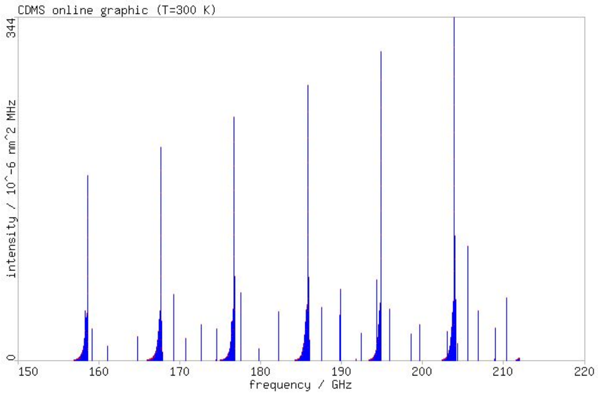

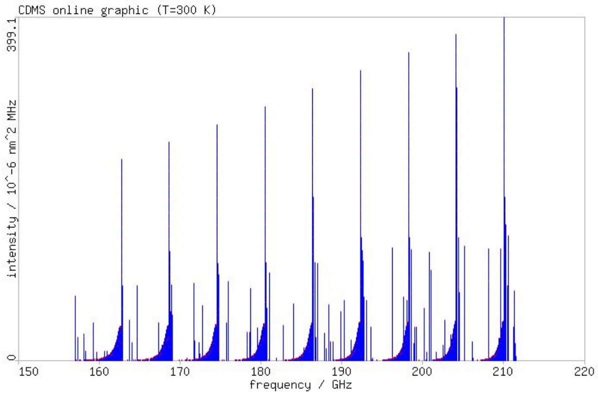

Projects in the mid-infrared

PAHs (Polycyclic aromatic hydrocarbons)

- 15% of the carbon in the interstellar medium (ISM) (Joblin et al. 1992)
- Dominant organic material (Ehrenfreund et al. 2006)
- 50% of the mid-IR luminosity (Li et al. 2004)
- Prebiotic role (PAH World) (Ehrenfreund et al. 2006)

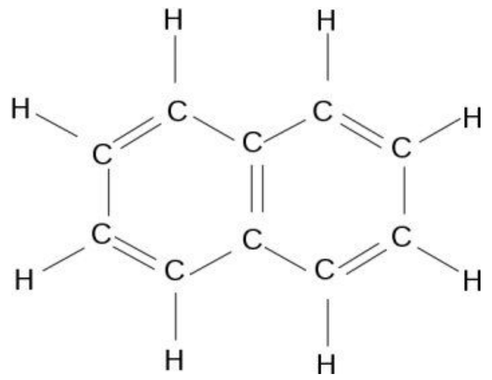

Naphthalene $C_{10}H_8$

PANHs (Polycyclic aromatic nitrogen heterocycles)

- Blueshift of the 6.2 µm band → PANHs
(Hudgins et al. 2005)

Class	6.2 μm	7.7 μm	8.6 μm
A	< 6.23	~ 7.6 ($F_{7.6}/F_{7.8} < 0.9$)	< 8.6
AB	——	($F_{7.6}/F_{7.8} = 1\pm0.1$)	——
B	$6.23 < \lambda < 6.29$	~ 7.8 ($F_{7.6}/F_{7.8} > 1.1$)	> 8.6
C	> 6.29	~ 8.22	——

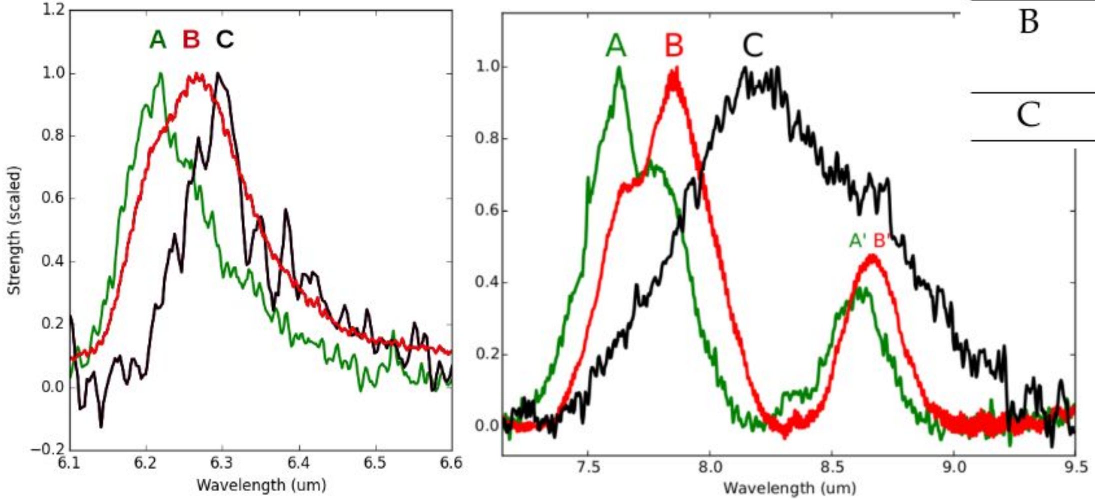

Fig.: General 6.2 µm profile variations for the classes A, B and C (E. Peeters et al. 2002)

PANHs in starburst-dominated galaxies

- Spitzer/IRS ATLAS project
  (Hernán-Caballero & Hatziminaoglou, 2011)

- Study of the 6.2 µm PAH band
  (Canelo et al. 2018)

- Comparison of the 6 - 9 µm PAH bands
  (Canelo et al. , in prep.)

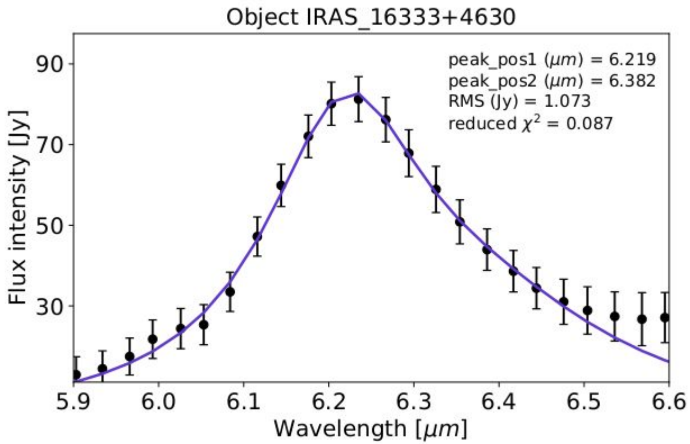

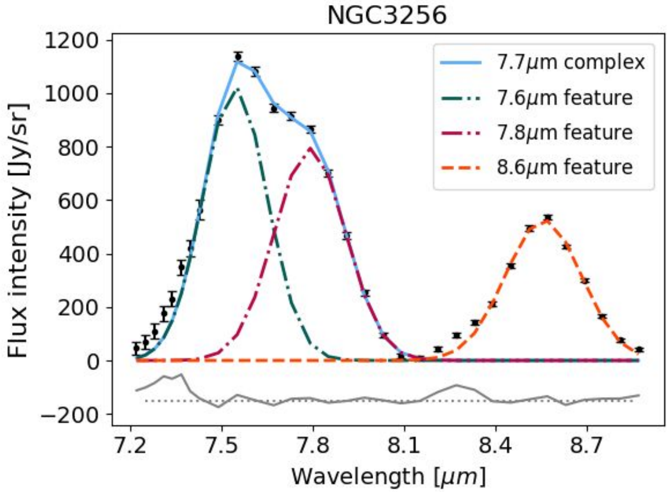

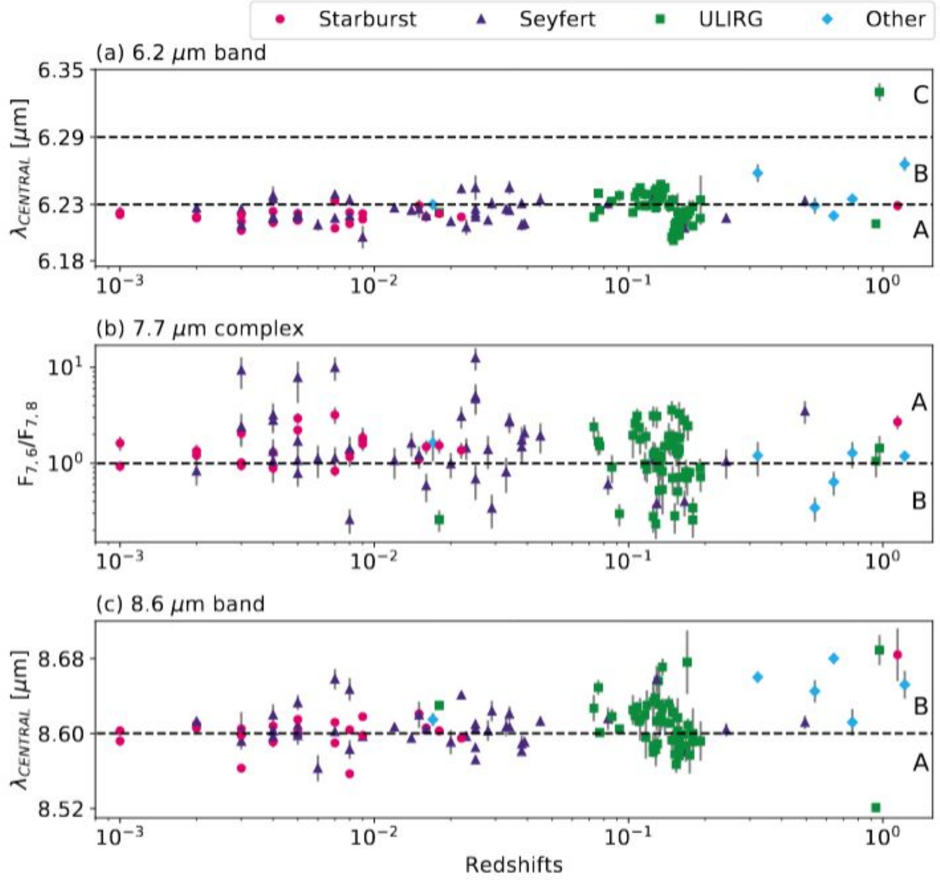

Figure 6. Distribution of the 6.2, 7.7 and 8.6 μm bands, respectively, according to the galaxies redshift. The dashed lines are the limits among the Peeters' classes, indicated also by A, B or C letter. The redshift axis is in logarithmic scale as well as the flux ratio axis in plot (b). The type of the galaxies were divided into four main groups and their data points are represented in the plots by different symbols. The uncertainties are displayed as grey error bars.

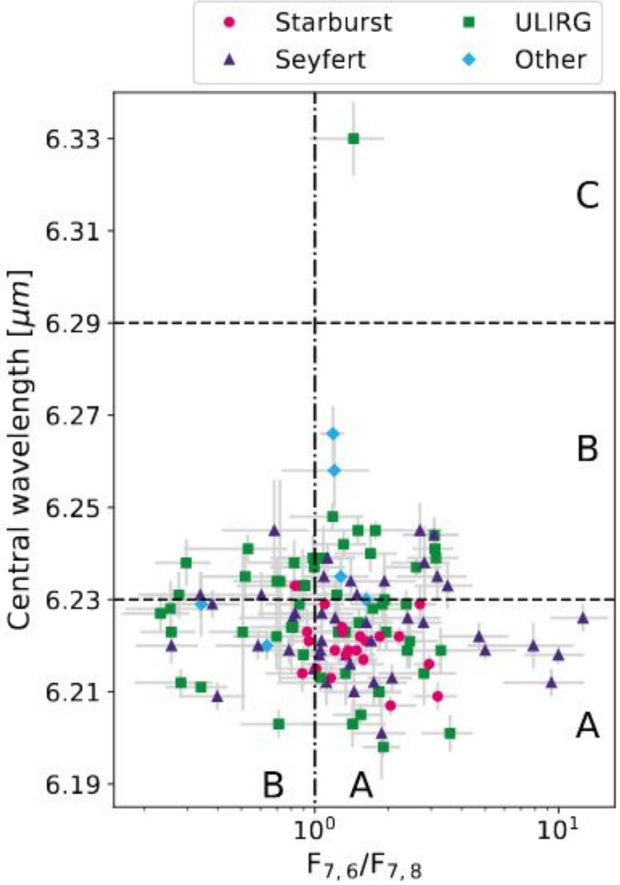

Figure 5. Relation between the flux ratio $F_{7.6}/F_{7.8}$ and the peak position of the 6.2 μm band.

Final remarks

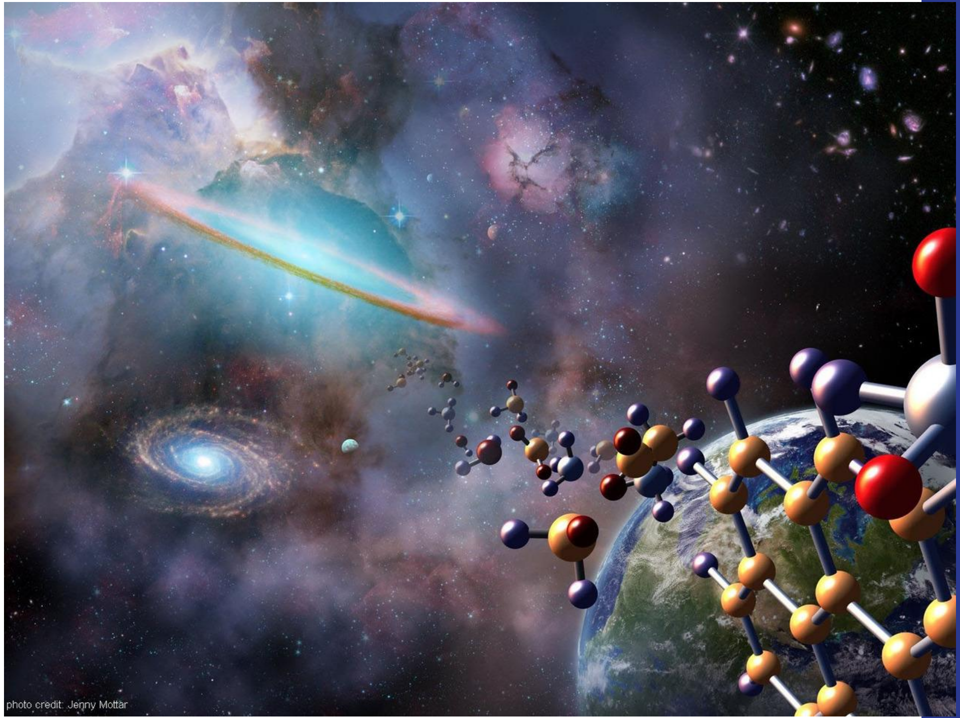

- Observation of important prebiotic molecules
- Development of chemical modelling
- Better understanding of the formation and abundance of N-heterocycles and their precursors

ALLAM 2019
Astrochemistry LLAMA Meeting

THANK YOU!

carla.canelo@usp.br

Astrochemistry Group @ IAG-USP

http://www.astro.iag.usp.br/~astroquimica/

Different densities

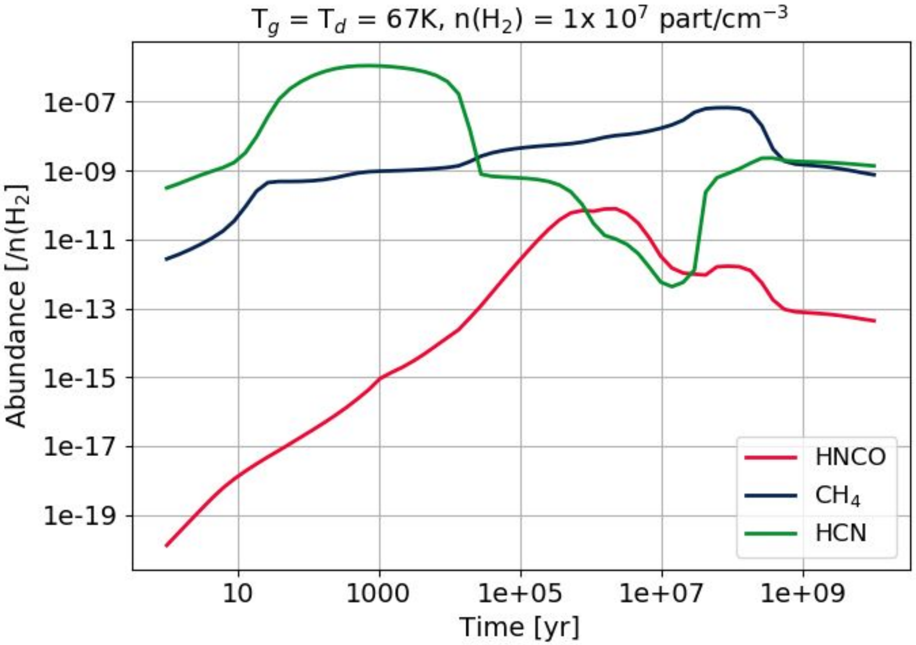

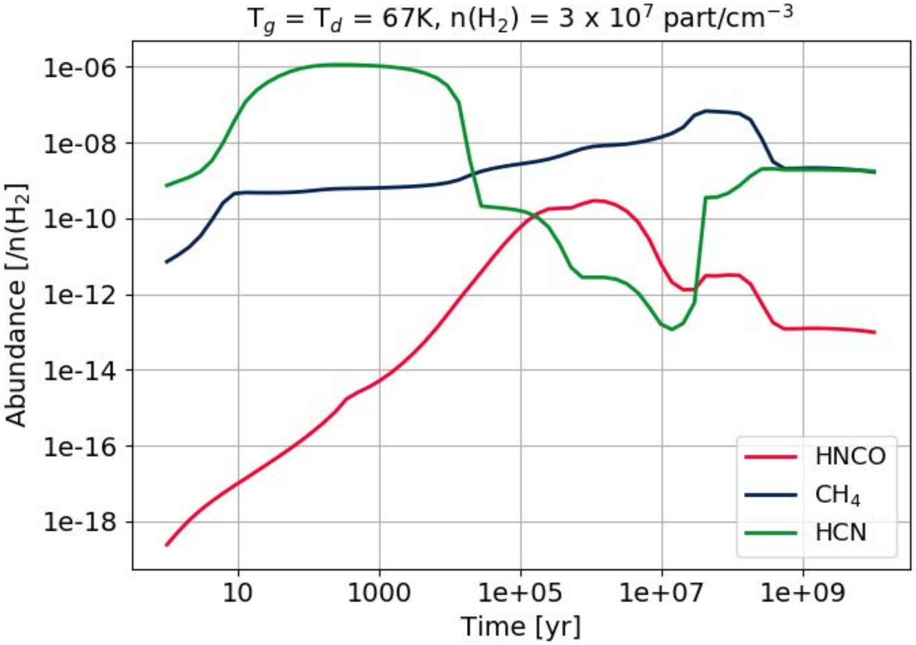

Different temperatures

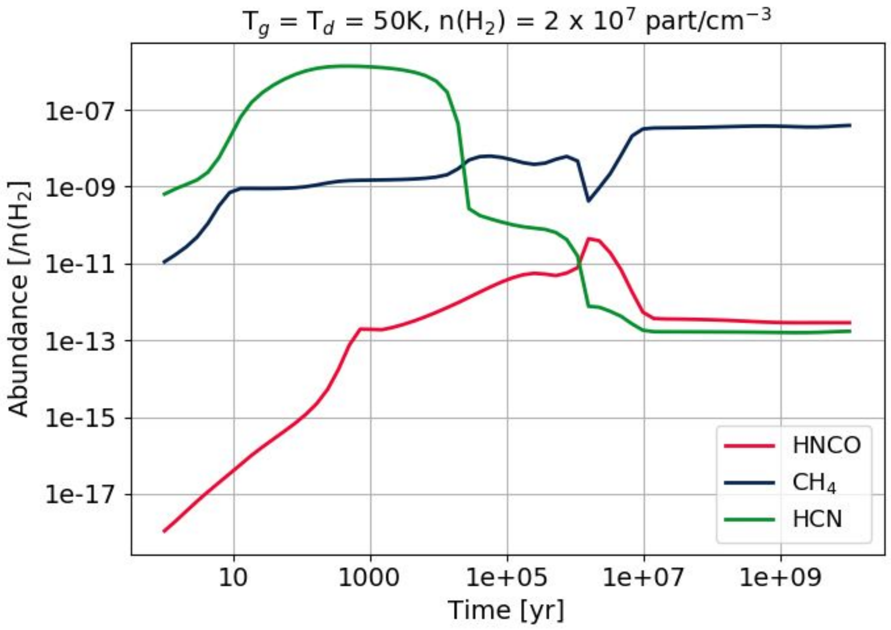

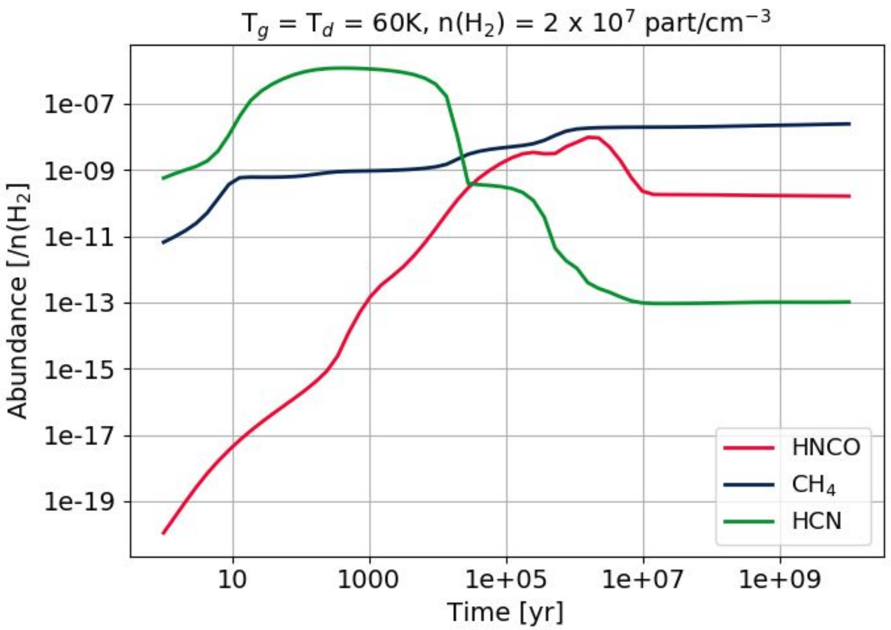

Different temperatures

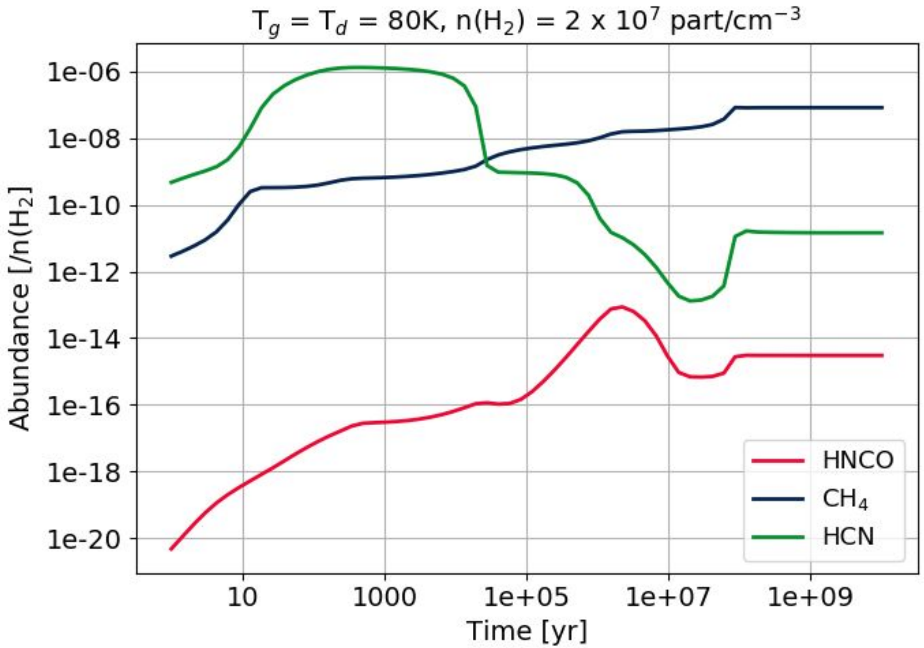

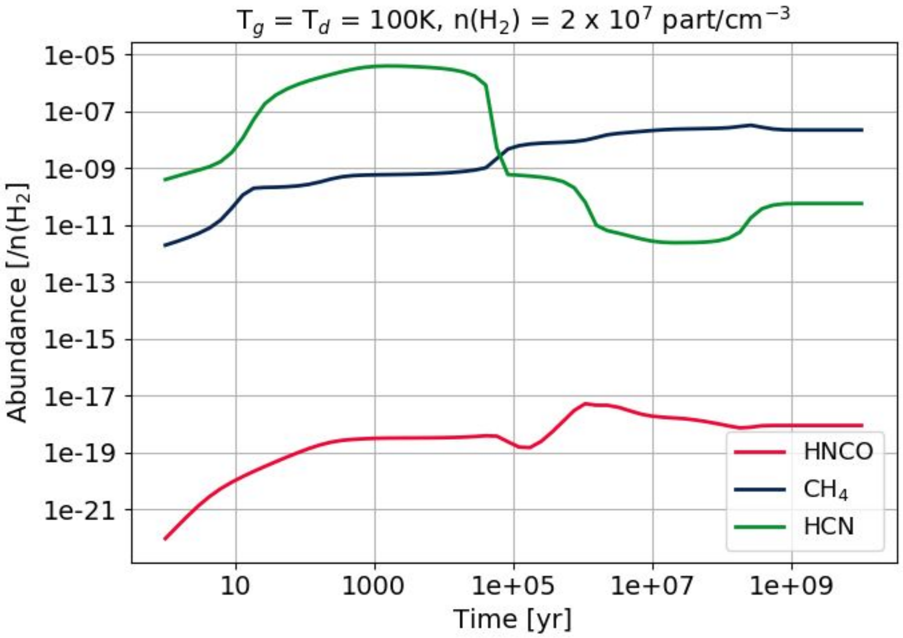

Small N-heterocycles

- Search for emission of minor units

pyrrole (C_4H_5N)

pyridine (C_5H_5N)

pyrimidine ($C_4H_4N_2$)

$C_4H_5N + CH \rightarrow C_5H_5N$

Source	N(pyridine) (cm^{-2})	N(quinoline) (cm^{-2})	N(isoquinoline) (cm^{-2})
IRC + 10216	7.9×10^{14}	1.2×10^{18}	2.8×10^{21}
	7.3×10^{12}	2.2×10^{13}	2.3×10^{14}
	8.6×10^{12}	1.2×10^{13}	6.2×10^{13}
CRL 618	2.5×10^{15}	1.9×10^{22}	3.3×10^{21}
	2.3×10^{13}	8.7×10^{13}	2.7×10^{14}
	2.7×10^{13}	1.6×10^{13}	7.2×10^{13}
CRL 2688	...	2.0×10^{18}	1.3×10^{21}
	...	3.6×10^{13}	1.1×10^{14}
	...	1.9×10^{13}	2.9×10^{13}

Tab.1: The derived upper limits for the molecular column densities (Charnley et al. 2005).

Formation of peptide-like molecules

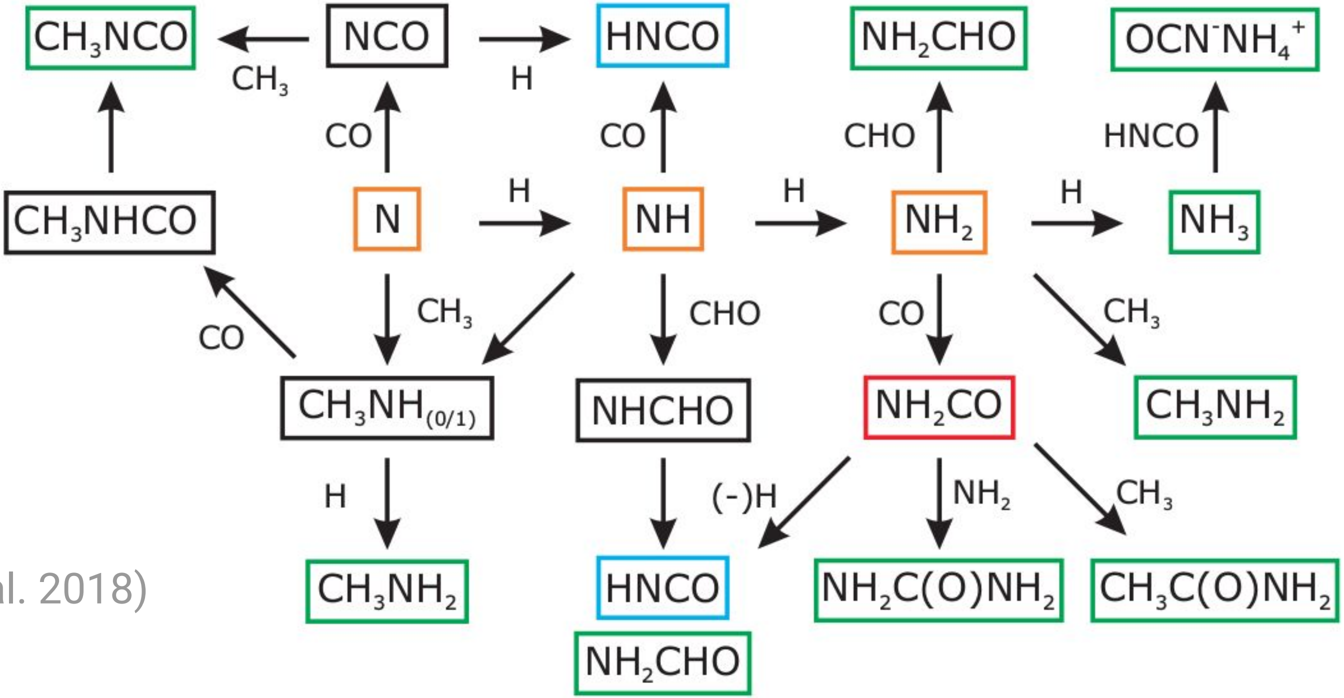

(Ligterink et al. 2018)

Figure 14. Proposed solid-state reaction scheme for the formation of the smallest generation of amides and CH_3NH_2, based on the findings of this work. The reactions derive from the nitrogen hydrogenation back bone (orange boxes). The green boxes indicate the products detected in the experiments, while the experimental precursor species HNCO is given in a blue box. $CH_3N_{0/1}$ indicates an intermediary product that is either the CH_3N or CH_3NH radical.

Data analysis

Fitting of the bands → scipy.curvefit

Gaussian profile

$$I_{gauss} = \frac{A}{\sigma\sqrt{2\pi}} exp\left(-\frac{(x-\lambda_c)^2}{2\sigma^2}\right)$$

- 6.2 µm (Canelo et al. 2018)
- 7.6 and 7.8 µm (Canelo et al. in prep.)
- 8.6 µm (Canelo et al. in prep.)

Integrated Gaussian fluxes

- 6.2 µm → 6.1 – 6.35 µm
- 7.7 µm → 7.2 – 8.2 µm
- 8.6 µm → 8.2 - 9 µm